DOI: 10.15201/hungeobull.75.1.1 Hungarian Geographical Bulletin **75** 2026 (1) 3–29.

Scenario-based analysis of the projected mean changes in the monthly frequency of hot days based on the latest CMIP6 simulations along European zonal segments

Ferenc Tamás DIVINSZKI[1], Anna KIS[1] and Rita PONGRÁCZ[1]

Abstract

The potential changes in extreme hot temperature (represented by TX35, i.e. the number of days with maximum temperature above 35 °C) are analysed, using the latest global climate model simulations ensemble mean of CMIP6, available in the new tool of the IPCC, namely, the Interactive Atlas. The analysis is carried out over Europe with a special focus on Central and Southern Europe. Our aim is to evaluate the spatial patterns within the projected changes in the period 2081–2100 that can be further used in several sectors, e.g. in the health sector, which is especially affected by the potential increase of extremely hot conditions. For this purpose, the projected changes of TX35 are compared to the reference-period 1995–2014 for four available scenarios from the newest scenario-family, namely, SSP1-2.6, SSP2-4.5, SSP3-7.0, and SSP5-8.5 representing different mitigation and adaptation challenges. As the projected increase is not limited to summer, the monthly-scale analysis is extended to the period from May to September. A novel approach is used to investigate the major factors in the projected changes, namely, six zonal segments are selected over Europe, covering the relevant parts of the continent with appropriate distances between them. The most important driving factors of the projected changes of TX35 are identified as follows: (i) the differences between regions due to their north-south or east-west locations (i.e. zonal and continental effects), (ii) elevation above sea level, (iii) the different anthropogenic effects (i.e. different scenarios). The results show that the key factor in the projected changes is the difference between anthropogenic effects. Furthermore, the sea-land surface differences also have substantial effect on the projected changes of TX35, especially in the southern regions. Continentality and elevation show only smaller effects overall.

Keywords: SSP scenarios, extreme temperature, IPCC Interactive Atlas, climate change, TX35, Europe, CMIP6

Received June 2025, accepted February 2026.

Introduction

With the intensifying global warming, both climate mitigation and adaptation have become key challenges (e.g. Rojas-Downing, M.M. *et al.* 2017; Eyring, V. *et al.* 2024). As warming intensifies, more frequent and more severe extreme events occur (Wobus, C. *et al.* 2018). A recent record breaking occurred on 22nd July 2024 that became the hottest day on Earth ever measured since the regular worldwide measurements started, as the daily global mean temperature reached a record of 17.16 °C (WMO 2025). Moreover, the year 2024 was the warmest year on record, with the global mean temperature exceeding the pre-industrial average by 1.6 °C (C3S 2025), and the previous record year (i.e. 2023) by 0.12 °C.

The consequences of such heat were damaging in many sectors. For instance, heat-related mortality rose above 40,000 cases in 2023, which is the second highest after 2022 (Gallo, E. *et al.* 2024). As even greater increase is projected in the frequency of extreme events, such risks are also expected to further increase in the future (Lüthi, S. *et al.*

[1] ELTE Eötvös Loránd University, Institute of Geography and Earth Sciences, Department of Meteorology, Pázmány Péter sétány 1/a, H-1117 Budapest, Hungary. Corresponding author's e-mail: pongracz.rita@ttk.elte.hu

2023). Another example can be mentioned in the agricultural sector, namely, the consequences of extreme weather events can cause serious food supply issues (Cogato, A. *et al.* 2019). Moreover, the energy sector is also vulnerable to these extreme heat events (Schaeffer, R. *et al.* 2012).

All these examples highlight the importance of the implementation of adaptation strategies. Our study assesses the current state-of-the-art projections of extreme temperature events, with the ultimate goal to support decision-makers in creating and optimizing long-term plans. It is important to provide detailed information of the consequences of non-acting in time. More specifically, the aims of this study are to answer the following questions: (i) What are the general spatial patterns of extreme temperatures over Europe? (ii) Are these patterns changing due to climate change, and do different anthropogenic effects (i.e. scenarios with different emission pathways) have an influence on these changes? (iii) What geographical effects are dominant in shaping the patterns of extreme temperatures in different parts of the continent? The novelties of the present study include the applied new scenarios, new climate model results, a newly available tool of the IPCC, and the monthly scale, which provides more detailed information for hot conditions than the usual, more general annual/seasonal scale. For these purposes global climate model simulations applying a new generation of scenarios are used, as finer resolution regional climate model simulations taking into account these scenarios are not available yet. Since temperature-related phenomena show usually less spatial variability than e.g. precipitation-related events due to their general statistical characteristics (Wilks, D.S. 2006), the resolution of global scale models is still sufficient for a robust assessment.

In the next section data and methodology used in this study are described. Then, the third section (Results) addresses the aforementioned questions by presenting and discussing the results of a systematic analysis. A comparison of the present study to other relevant studies can be found in the fourth section (Discussion), and finally, the conclusions are summarised.

Data and methodology

The assessment reports (AR) published by the IPCC have been the key information source of climate science for the last few decades. The recently published AR6 (IPCC 2021) contains the results from the latest climate model simulations in the framework of CMIP6 (Eyring, V. *et al.* 2016), with the future projections taking into account the new SSP-scenarios (O'Neill, B.C. *et al.* 2017) paired with the previous RCPs (van Vuuren, D.P. *et al.* 2011) used in AR5 (Taylor, K.E. *et al.* 2012). The available data were then assembled in the Interactive Atlas (IA) (Gutiérrez, J.M. *et al.* 2021).

The IA provides an easy-to-use interface, where the different databases, scenarios etc. can be compared by using various diagrams, graphs, and maps. However, there are only limited options to perform scientific studies unless using the built-in option to download multi-model mean data for different datasets, different scenarios, several climate variables/indices, and time periods. Besides the more general approach using the entire year, it is also possible to focus on a specific season or month, so the annual cycle can also be evaluated from the climate change viewpoint.

In this study, multi-model monthly mean (each member has an equal weight) data were downloaded for all the four available SSP-scenarios, SSP1-2.6, SSP2-4.5, SSP3-7.0, and SSP5-8.5. The list of the individual models is shown in *Table S1* (Supplementary section).[2] Altogether 22 models provide simulation for all the four scenarios, in addition, 6 models were simulated only for two or

[2] Note, that the downloading is possible only for the multi-model ensemble mean and not the individual simulation results, thus, the inter-model spread and the ensemble uncertainty cannot be assessed; moreover, the changes are shown as a multi-year average without the time series of each annual value.

three scenarios. Both the SSP2-4.5 and SSP5-8.5 ensembles contain 27 model simulations. However, these differences of a few model simulations within the scenario-ensembles do not affect the mean results.

To study the effects of extreme heat, the focus of this study is on the climate indicator called 'days with maximum temperature above 35 °C' (indicated as TX35) by 2081–2100. The target period of projections is selected according to the most recent IPCC AR (2021), to ensure the greatest climate signals of the various scenarios by the end of the 21st century (called long term by IPCC [2021]). The projections are compared to the 1995–2014 reference period, which covers the last 20 years of the historical simulations prior to starting the scenario runs from 2015.

To cover Europe entirely, five zonal segments are selected from the Northern Hemisphere, i.e. 37.5°, 42.5°, 47.5°, 52.5°, and 57.5° (*Figure 1*), each segment represents a series of grid cells along the corresponding 1° latitude zone, e.g. the zonal segment of 37.5° represents the zone between 37° and 38°. However, the downloading process does not allow the users to select a desired area or certain grid cells to receive data from, the netCDF file of the entire global field has to be downloaded. The downloaded files contain the multi-model mean values of the entire ensemble for the target period for each month separately, but not for each simulation individually. Therefore, first, the non-European grid cells are eliminated by applying a European land contour mask to the global coverage, and then, the appropriate target segments are cut from these global data series. After re-gridding all individual simulations (the finest with a horizontal resolution of 0.5° × 0.5°, while the most coarse simulation with 2.81° × 2.77°, but the majority is closer to 1° × 1°) to a uniform custom grid (Gutiérrez, J.M. *et al.* 2021), the horizontal resolution of the multi-model ensemble mean is 1 × 1° that finally resulted in 32 (from 9°W to 23°E), 37 (from 9°W to 28°E), 47 (from 2°W to 48°E), 55 (from 10°W to 45°E), and 51 (from 7°W to 44°E) grid cells, respectively, along the segments from the southernmost (37.5°N) to the northernmost (57.5°N). Each segment begins from the westernmost land-covered grid cell near the Atlantic Ocean, and then, all the inner water-covered grid cells are kept along the segment until reaching the Aegean Sea, the Black Sea, or the river Volga in the east.

Then, the simulated data are assembled to special diagrams and graphs systematically, to help visualise and analyse the massive amount of information. Three types of diagrams are created: (i) The projected increase of TX35 is displayed for the four scenarios across the segments, with a grey shading showing the elevation of the grid cells so sea-land differences (i.e. the value of 0 m as elevation and the longitudinal location together define sea areas) can be compared from south to north. In addition, the continentality can be assessed on the basis of longitude, from west to east, as moving away from the Atlantic Ocean. (ii) The projected changes are shown as a function of elevation to analyse the orographic effect. The interpretation is based on visual and/or qualitative assessment, therefore, this applied methodology does not allow for a strict statistical separation of elevation and continentality effects. (iii) The projected warmings for the three SSPs with different mitigation/adaptation challenges are compared to the projections of SSP1-2.6 with strong mitigation and adaptation introducing as soon as possible (i.e. representing the goals of the Paris Agreement, and considered as a baseline scenario), so the anthropogenic effect as well as the impact of its reduction can be evaluated. In addition, the correlation coefficients between the monthly zonal patterns of SSP1-2.6 and the other SSPs are tested for significance using t-test (at the significance level 0.05).

To ensure full coverage of substantial increase in TX35 over the year, apart from the three summer months, results for May and September are also analysed. This is expected to be an important extension in the southernmost segments, where the increase in TX35 is still substantial before and after the summer months. Note that the analysed month

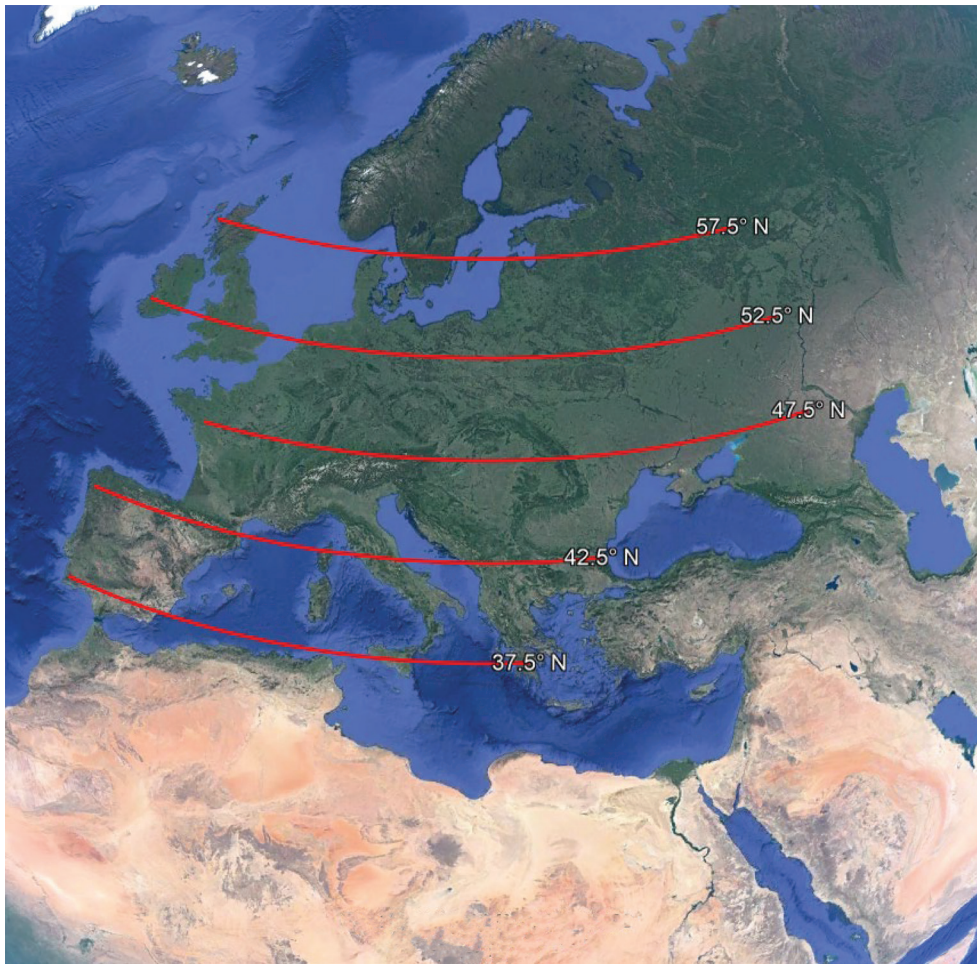

Fig. 1. Location of the selected five zonal segments in Europe. *Source*: Data SIO, NOAA, U.S. Navy, NGA, GEBCO Image Landsat / Copernicus Image IBCAO.

always provides an upper limit to the TX35 values, i.e. the total number of days of the given month. Therefore, if the values are already high in the historical period (i.e. hot conditions are quite frequent historically, shown in *Figure S1* [Supplementary section]), the possible increase is limited. However, if the values are low in the reference period (i.e. moderate/cool climatic conditions are currently present), a greater potential increase is possible. Hence, if the index values reach the upper limit (i.e. the maximum temperature will be above 35 °C every day of the month) for both cases, the latter will suffer from the higher increase only because of the lower reference value.

Results

The projected monthly increase of TX35 is analysed across the 37.5°N, 42.5°N, 47.5°N, 52.5°N and 57.5°N segments, respectively, for the period May–September (diagram

type (i)). Then, the diagram type (ii) shows the projected changes in TX35 as the function of elevation. The five segments form two major groups. Group1 consists of the 37.5°N, 42.5°N and 47.5°N segments where high elevation areas with peaks are close to 1500 m. Group2 is formed by the remaining two segments: 52.5°N and 57.5°N, where the elevation is below 400 m at any longitude.

Finally, the diagram type (iii) analyses differences between scenarios instead of other geographical-location-determined climatic effects. For this purpose, the most sustainable scenario, SSP1-2.6 serves as a basis, to which all the others are compared in order to analyse the adaptation and mitigation effects on the changes of TX35. First, the correlation coefficients between the spatial patterns of SSP1-2.6 and the other SSPs along each zonal segment are tested for significance and show significant similarities (i.e. the correlation coefficients are between 0.65 and 0.99, except the 57.5°N segment, where only minor changes are projected, and the coefficient values range between 0.75 and 0.99 (*Table S2*) (Supplementary section). These imply that the spatial patterns of the SSPs are very similar at every segment, the main difference between the scenarios is the magnitude of the projected increase in TX35. These are highlighted by green dotted lines on the corresponding graphs, with the projected increase being the same, two-fold, and four-fold compared to the SSP1-2.6 scenario.

Along the 37.5°N segment (in *figures 2–4*), the TX35 values in the reference period are already high due to the southern location. Therefore, the projected increase for the 2081–2100 target period is not the greatest among the segments. However, it is still significant, especially in July, August, and September (*Figure 2, c, d*, and *e*, respectively), when the overall relative increase over land is 30–50 percent and more than 80 percent in the case of SSP1-2.6 and SSP5-8.5, respectively. In fact, the land areas of southern Spain, Italy and Greece are projected to warm much more compared to water surfaces, so higher increase of TX35 is likely to occur by late-century. This spatial pattern is also visible in the reference period; hence, the general spatial pattern will not change according to any projection either. However, the spatial differences between the land areas and water surfaces are likely to increase.

There are grid cells with elevation close to 1000 m (*Figure 3*), which makes this latitude segment belong to the same group as 42.5°N and 47.5°N, where peaks can reach up to 1500 m. The general pattern is similar in every month: there are three maximum increases for all four scenarios, at around 200 m, at 450 m, and at 800–1000 m a.s.l., which are the respective elevations for Sicily, Peloponnese, and the Iberian Peninsula. These imply that elevation does not influence much the projected change of TX35. However, as this latitude crosses the Mediterranean Sea and every land grid cell is close to the Mediterranean Sea, the effects caused by the elevation differences are dominated by a more important and stronger effect, i.e. the distance from extended water surfaces. The moderating effect of sea cover is especially highlighted in June and September (*Figure 3, b*, and *e*). For instance, in *Figure 3, e* the greatest increase projected at the water grid cells (0 m elevation) is 2.7 days, whereas it is just below 2 weeks at the land grid cells based on the SSP5-8.5 scenario. On the other hand, the difference between these grid cells is reduced in July and August to 5 days (see *Figure 3, c*, and *d*, respectively).

The scenarios show different magnitudes of increase in different months (*Figure 4*). On the basis of the calculated linear regression coefficients for the three scenarios, a general pattern is shaped across the months. The largest coefficient values can be identified in May, namely, 2.5, 5.5 and 7.7 for SSP2-4.5, SSP3-7.0 and SSP5-8.5, respectively, indicating the ratio of the mean projected increases compared to SSP1-2.6. The coefficients reduce from May to July and further to slightly less than 2 in August, when the differences between the scenarios disappear in terms of the overall fitted linear regression. This is mostly due to a spatial difference occurring

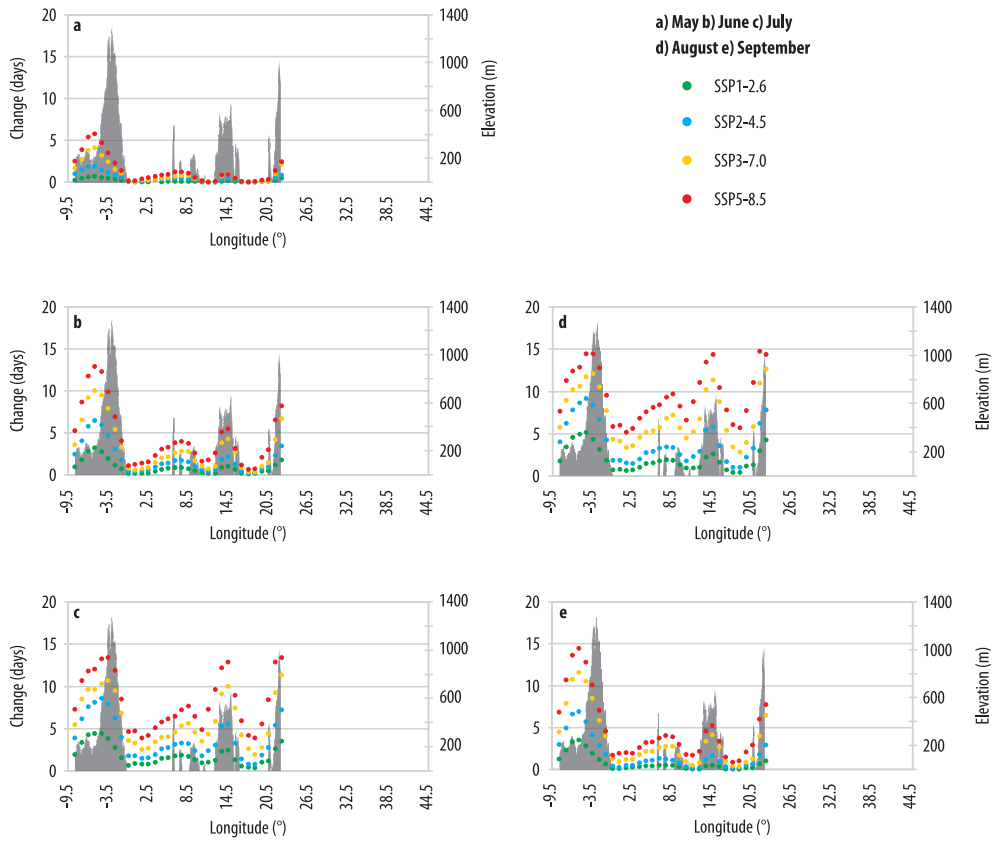

Fig. 2. Projected monthly changes of TX35 (2081–2100 vs. 1995–2014) for SSP1-2.6, SSP2-4.5, SSP3-7.0, SSP5-8.5 and elevation along the zonal segment of 37.5°N. *Source:* Authors' own elaboration.

in the segment, namely that if the projections for water and land surfaces are separated, then the different scenarios have different coefficients for these two surface types. More specifically, the coefficients for land surfaces are 1.1 and 1.08 for the SSP3-7.0 and SSP5-8.5 scenarios in August, whilst for water surfaces, they are 2.8 and 3.1, respectively. Then, the regression coefficients increase again in September; however, they still do not reach the values in May. Note that the smallest increase in monthly TX35 is found in those months when the coefficients are the largest (i.e. in May and September). Therefore, the greater the projected increase, the more reduced the relative differences between the scenarios are.

Moving northward to the *42.5°N* segment (*Figure 5*), the aforementioned spatial patterns are even more pronounced than along the 37.5°N segment. The differences are the most remarkable in August (*Figure 5, d*), and almost as much in July (*Figure 5, c*). The increase of 18.4 days in the grid cell with the centre of (42.5°N, 25.5°E) in August is the highest among every zonal segment. However, in the same month, along the same latitude but at the 5.5°E longitude, the projected increase is only 3.3 days. Both changes are projected for the SSP5-8.5, the scenario with high challenges in mitigation, low challenges in adaptation, with the highest radiative forcing change of 8.5 W/m^2 among the analysed scenarios. The changes projected by the

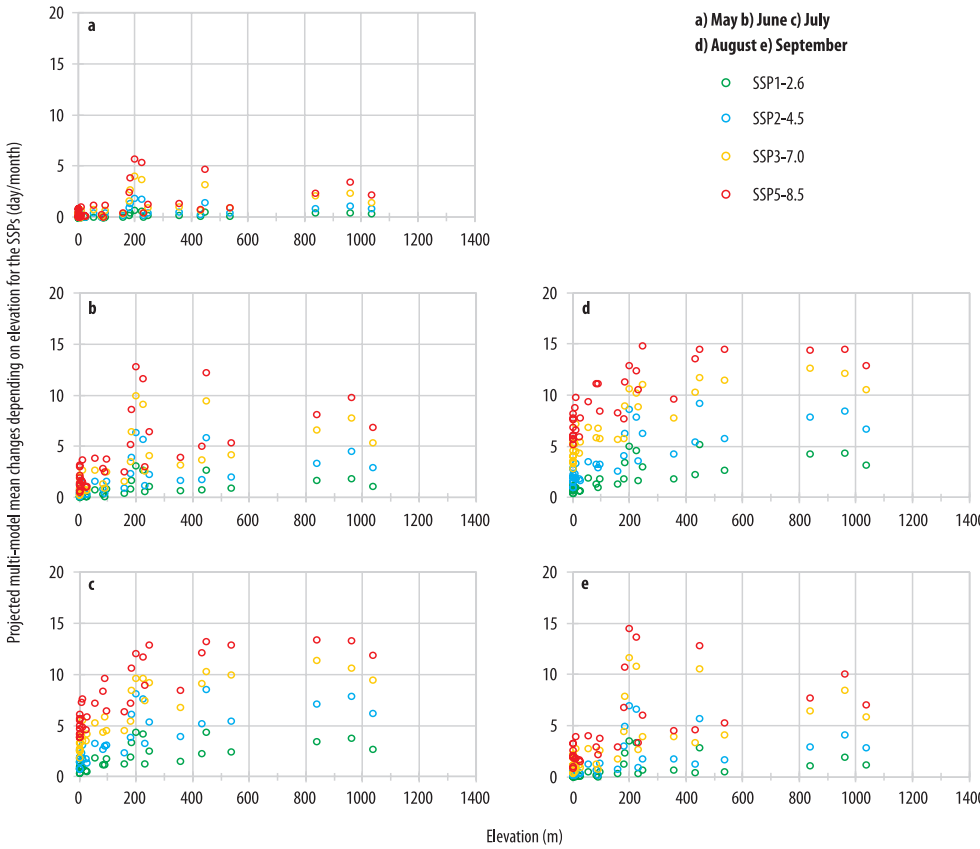

Fig. 3. Projected monthly changes of TX35 (2081–2100 vs. 1995–2014) depending on elevation at 37.5°N for SSP1-2.6, SSP2-4.5, SSP3-7.0 and SSP5-8.5. *Source:* Authors' own elaboration.

SSP1-2.6 scenario with the lowest radiative forcing change show similar spatial patterns, the increase is the greatest at 25.5°E, and the smallest at 5.5°E, however, with much lower increases, i.e. less than 4 days for the 22.5°E, and 0.2 days for the 5.5°E. Therefore, it can be concluded that the direction of the projected change of the TX35 and the spatial patterns along the segments are similar regardless the scenario. The difference is the magnitude of the projected increase, which shows that the higher the radiative forcing becomes, the greater the spatial differences (especially between land and sea). Besides the land vs. sea difference, an overall greater increase tends to be projected over land areas as moving toward east, implying a continental effect.

Analysing the effects of elevation, *Figure 6* shows that the 42.5°N segment has a much more diverse terrain than the 37.5°N segment, with grid cells being spread almost evenly within the interval of 0–1400 m elevations. The months again show similar patterns compared to each other; however, the differences across the different elevations are the most pronounced in July (*Figure 6, c*) and August (*Figure 6, d*), when the projected increase is the highest. The greatest increase is projected to occur at around 400 m above sea level, namely, more than 18 days in August, based on the SSP5-8.5 scenario. The smallest projected increases can be recognised in two different levels: (i) at the water-covered grid cells and the low elevation areas representing

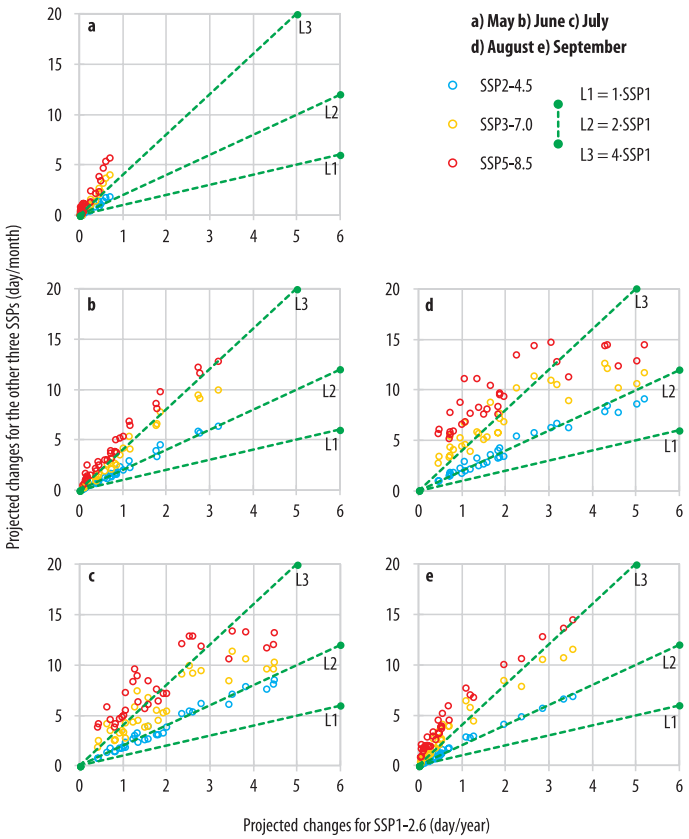

Fig. 4. Projected monthly changes of TX35 (2081–2100 vs. 1995–2014) for SSP2-4.5, SSP3-7.0 and SSP5-8.5 compared to SSP1-2.6 at 37.5°N. *Source:* Authors' own elaboration.

the shoreline lands, and (ii) at the highest elevation points around 1300 m above sea level. Here, the absolute smallest increases belong to category (i). Note that this is a general spatial distribution in the increase of TX35 for all the four scenarios, however, the actual value of the projected change is different. The lower the projected increase is, the less the influence of elevation. Similar patterns can be seen in the case of May and September (*Figure 6*, *a*, and *e*), when the increase is also smaller, therefore, the differences caused by elevation are not present so clearly. Also, the projections of the four scenarios are close to each other implying smaller effect from the general global warming rate (which is strongly depending on the radiative forcing change).

As for the inter-scenario comparison relative to the SSP1-2.6 scenario (*Figure 7*), there are similar patterns across the months to the 37.5°N segment, however, here, May (*Figure 7*, *a*) is more similar to the summer months, and only September (*Figure 7*, *e*) is substantially different from them. This is also reflected by the regression coefficients, which are within a narrow range from May to August (1.5-2 for SSP2-4.5, 3-3.4 for SSP3-7.0, and 3-4.5 for SSP5-8.5), but differ from these in September (2.5 for SSP2-4.5, 5.5 for SSP3-7.0, and 7.1 for SSP5-8.5). It is also worth noting that the projections for the grid cells form two major

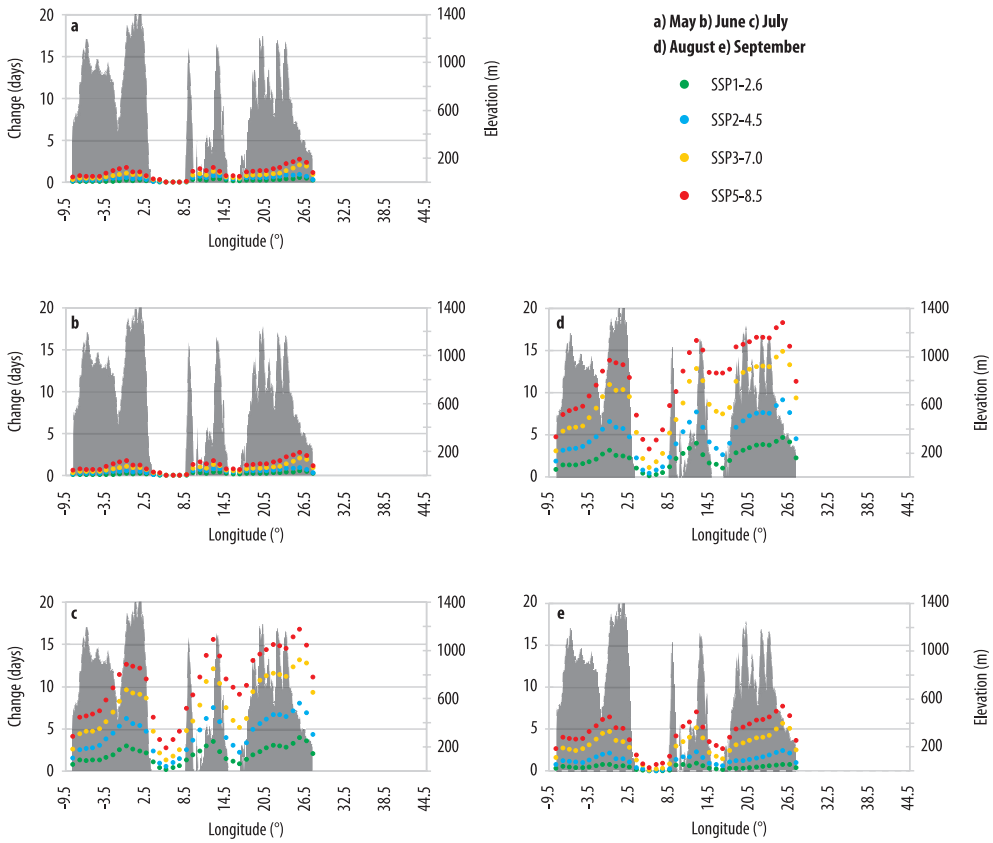

Fig. 5. Projected monthly changes of TX35 (2081–2100 vs. 1995–2014) for SSP1-2.6, SSP2-4.5, SSP3-7.0, SSP5-8.5 and elevation along the zonal segment of 42.5°N. *Source:* Authors' own elaboration.

clusters on the diagrams for the 37.5°N segment due to the limited land areas, especially in June and September (see *Figures 4, b*, and *e*), whereas at the 42.5°N segment, the points are scattered evenly along a fitted regression line on the basis of all longitudes.

Compared to the two southern segments, the continental effect is much stronger at the *47.5°N* segment (*Figure 8*). The more eastern a grid cell is, the further it is located from the Atlantic Ocean, and therefore, the projected increase is higher. Note however, that in July and August (*Figure 8, c*, and *d*), the intra-zonal increase stops from the 30.5°E towards the eastern end of the segment. This is due to the effects of the other large body of water, i.e. the Black Sea, which is lying just south of the 47.5°N segment and moderates the effects of the growing distance from the Atlantic Ocean. Furthermore, other features also shape the spatial patterns, namely, two large mountain ranges, the Alps and the Carpathians. Therefore, the complex effects of continentality and orography determine the overall intra-zonal and inter-scenario characteristics.

The effects of the orography are visualised in *Figure 9*. As expected, the greatest increase (i.e. more than 2 weeks) is linked to the lower, plain areas for every month. From around 100 m a.s.l. to 800 m, the projected change of the TX35 decreases almost linearly. However, this is abrupted by a secondary maximum

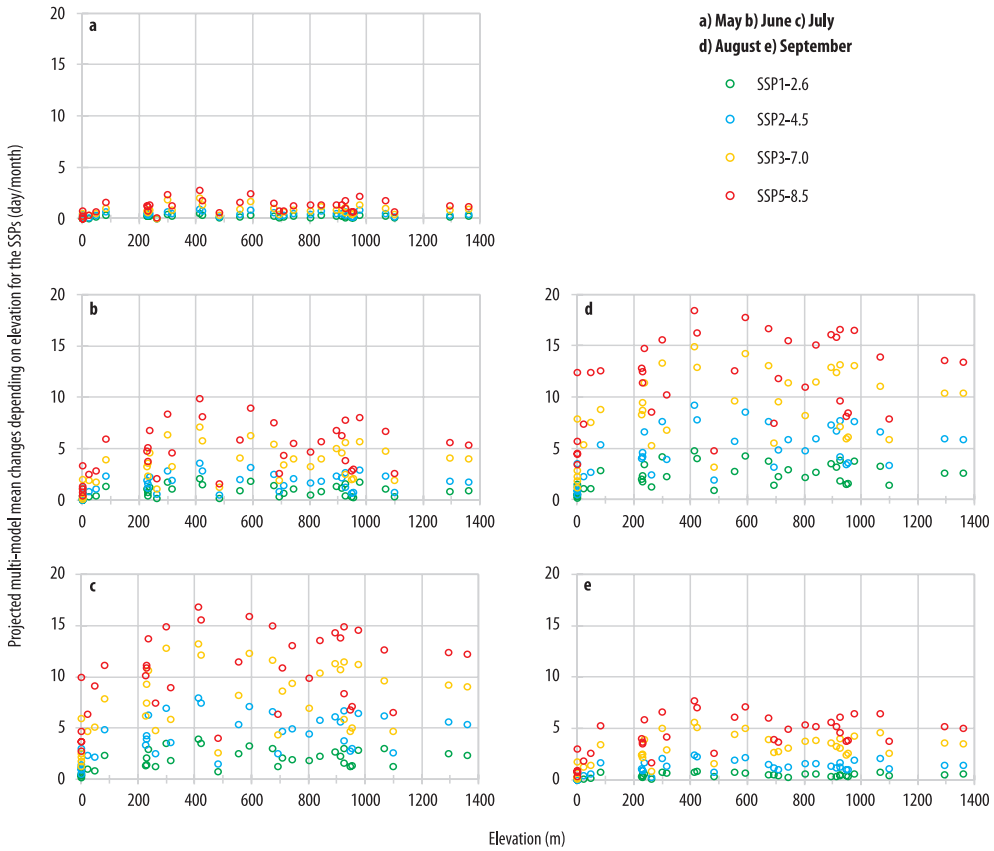

Fig. 6. Projected monthly changes of TX35 (2081–2100 vs. 1995–2014) depending on elevation at 42.5°N for SSP1-2.6, SSP2-4.5, SSP3-7.0 and SSP5-8.5. *Source:* Authors' own elaboration.

of the TX35 increase between 800 m and 1000 m, comparable to the values at 300–400 m (*Figure 9, b, c,* and *d*). The reason behind this pattern is the geographical location of the grid cells with the 800–1000 m elevation. They belong to the Carpathians, which are located on the eastern parts of the segment, thus, in addition to the orography, the continental effect also influences the projected increase of monthly TX35. Note that this pattern is more pronounced from June to August (see *Figure 9, b, c,* and *d*) and completely disappears in May (*Figure 9, a*) due to the very small projected changes at the beginning of the summer half-year. As the values of monthly TX35 in the historical period were a lot lower in the mountain areas than in the plain areas *(Figure S1)* (Supplementary section), the already existing spatial differences are likely to increase in the summer months and probably not to change in May and September for the target period 2081–2100.

As for the scenario comparisons, similarly to the 37.5°N segment, some specific points also form clusters along the 47.5°N segment (*Figure 10*), namely, in June and August (*Figure 10, b,* and *d*). However, in this case the fitted linear regressions between the projected increases of the SSP1-2.6 and the other two scenarios (SSP3-7.0 and SSP5-8.5), are more relevant for the separate clusters than in the case of the other segments. This

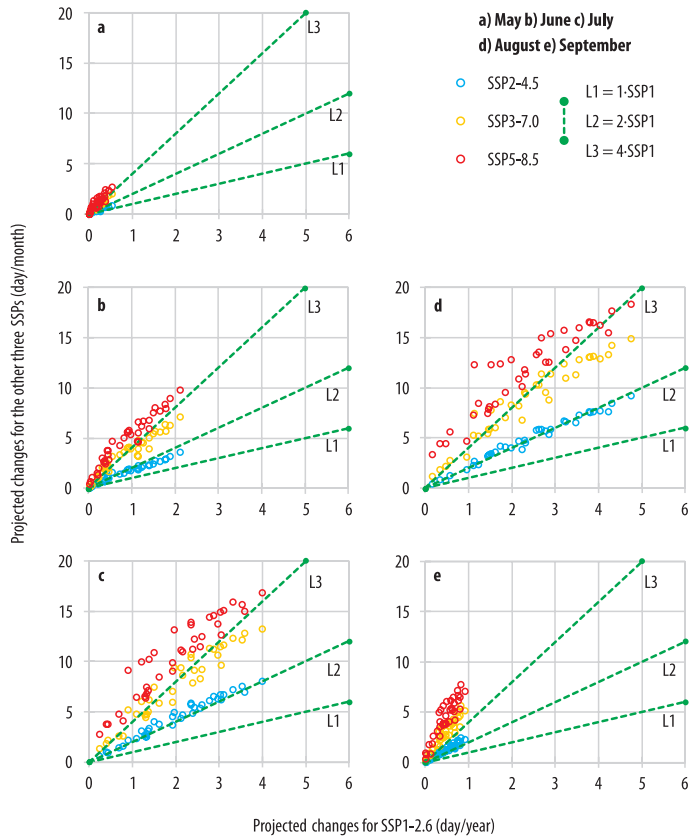

Fig. 7. Projected monthly changes of TX35 (2081–2100 vs. 1995–2014) for SSP2-4.5, SSP3-7.0 and SSP5-8.5 compared to SSP1-2.6 at 42.5°N. *Source:* Authors' own elaboration.

implies for example for August, when the regression coefficients for all the points are 2.3 for SSP3-7.0, and 2.6 for SSP5-8.5, whereas without the easterly longitudes, the coefficient values would be higher (i.e. 3.1 and 3.6, respectively). So based on *Figure 10, d*, the relative differences are far greater between the scenarios if only the first cluster is analysed (at around 0-2 days of increase in TX35 based on the SSP1-2.6) and much smaller if only the second. To reveal the reasons behind, the segment was cut into two smaller parts, a western and an eastern segment. This was due to the characteristics of the 47.5°N, as the growing continentality effect from west to east is highly influential in creating the spatial patterns. Similar diagrams are created for both subsegments, and the results show that the points in cluster1 almost entirely belong to the western part of the segment, and the points in cluster2 belong to the eastern part of the segment. The clustering can match the subsegments if the entire zonal segment is separated to the following two subsegments: (i) grid cells located west to the Alps and in the Carpathians (cluster1), (ii) grid cells located east to the Alps, except for the Carpathians (cluster2). This shows that the relative location to the Alps is a key factor when evaluating the projections. The location also explains the lower increase ratio of the higher radiative forcing change sce-

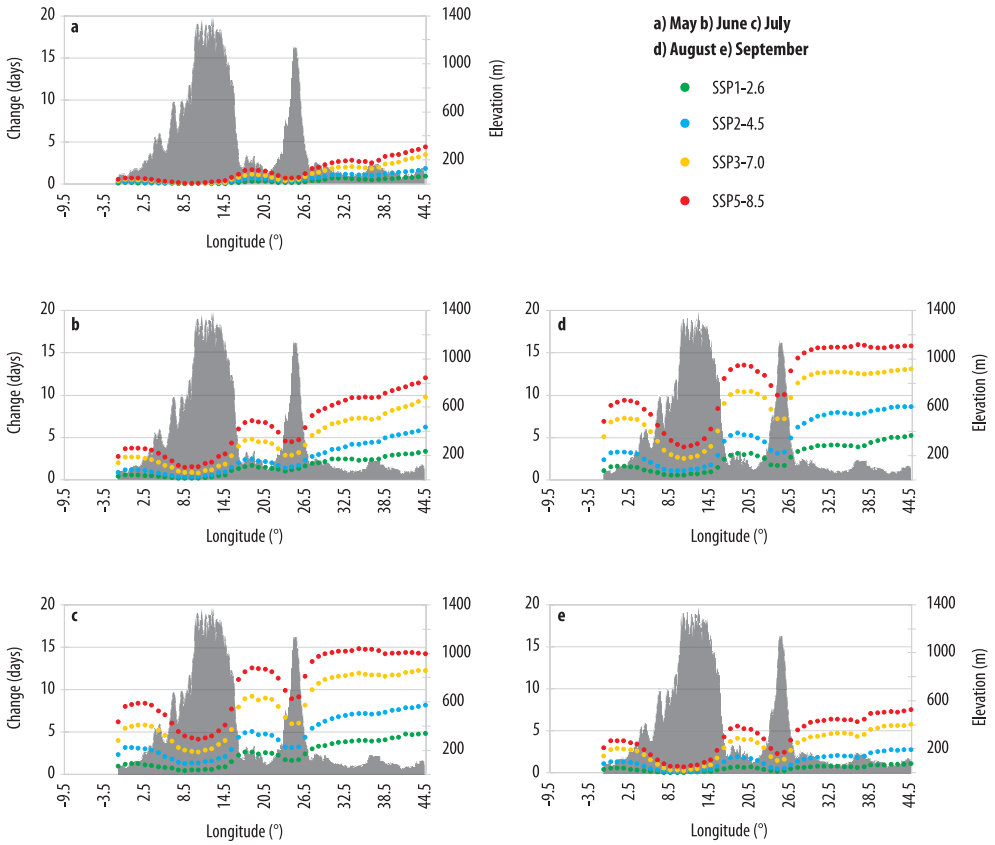

Fig. 8. Projected monthly changes of TX35 (2081–2100 vs. 1995–2014) for SSP1-2.6, SSP2-4.5, SSP3-7.0, SSP5-8.5 and elevation along the zonal segment of 47.5°N. *Source:* Authors' own elaboration.

narios relative to the SSP1-2.6 in cluster2. In these areas, especially in the east, the values of monthly TX35 were already high in the reference period (*Figure S1*) (Supplementary section). Hence, the physical upper limit of these values (20–23 days/month for SSP3-7.0 and 25–27 days/month for SSP5-8.5) driven by the added forcing levels and affected by the Black Sea, will be reached in July and August (*Figure 10, c*, and *d*) based on the high radiative forcing change scenarios.

Moving northward to the *52.5°N* segment (*Figure 11*), the greatest number of grid cells are analysed among all the latitudes. This is due to the selection process, where the main aim was to ensure that the majority of the grid cells are covered by land. Due to its northern location, the projected increase along this segment is generally lower than in the more southern segments. However, a considerable increase is projected in the eastern parts of the segment in the summer months, and an increase of up to 10 days will be likely possible based on the SSP5-8.5 scenario. The most dominant effect here is continentality, which can be explained by the facts that (i) the water surfaces are only located in the western part of the segment, and do not cover many grid points unlike along the 37.5°N and 42.5°N segments; and (ii) the 52.5°N segment lacks higher elevation areas, unlike the 47.5°N segment. As a consequence of all these, the

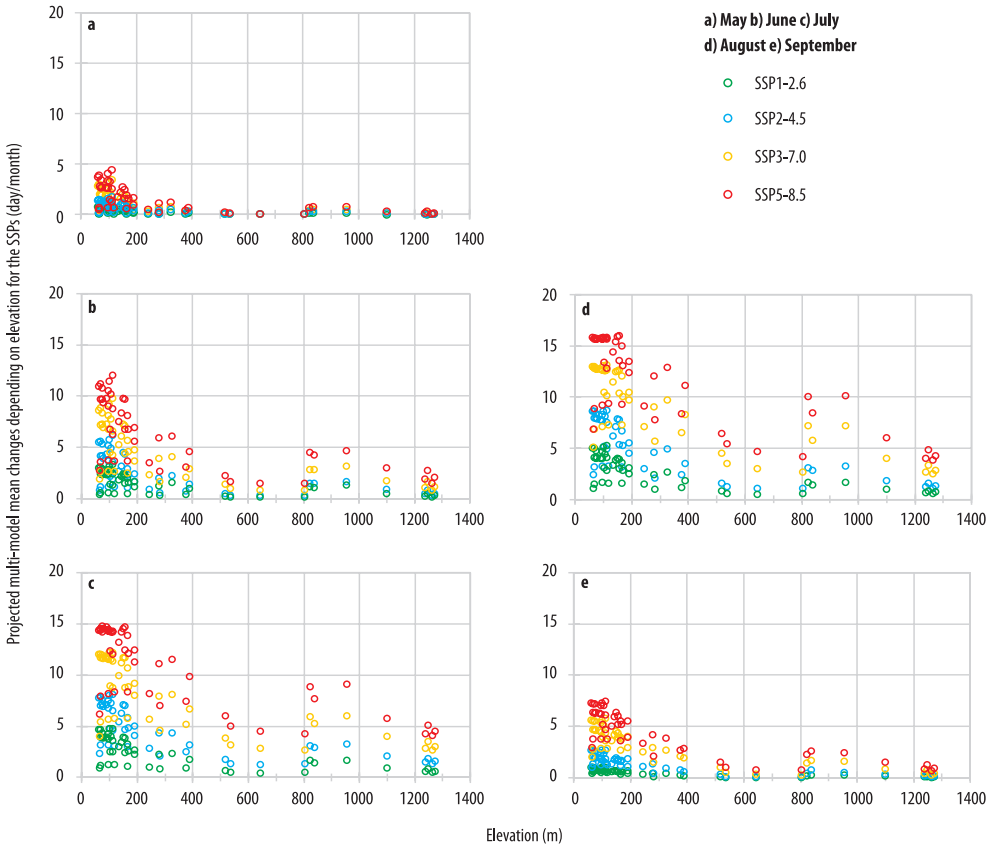

Fig. 9. Projected monthly changes of TX35 (2081–2100 vs. 1995–2014) depending on elevation at 47.5°N for SSP1-2.6, SSP2-4.5, SSP3-7.0 and SSP5-8.5. *Source:* Authors' own elaboration.

greater increase in TX35 with increasing elevation (*Figure 12*) is solely due to the higher elevation areas being in the eastern part of the segment, especially in June, July and August.

Continentality also clearly appears on the diagrams in *Figure 13*, especially for the three summer months. Note that the increase is very small in the western parts of the segment for every month, whereas an increase up to 10 days/month is projected in the east in August when SSP5-8.5 is taken into account (*Figure 13, d*). The regression coefficients are the smallest in June for all scenarios, which is different from the southern segments where the minimum was projected in August.

Finally, at the most northerly segment, at *57.5°N* (*Figure 14*), the very slight changes in the monthly TX35 are limited to the summer months only, from which the highest projected changes can be identified in July (*Figure 14, c*). This is different from the more southern segments, where the highest increase is projected in August (with much more substantial increases anyway than at the 57.5°N segment). Similar to 52.5°N, there are no high elevation areas along the segment (*Figure S2*) (Supplementary section), therefore, continentality has the major effect on the spatial distribution. The regression coefficient values show similar pattern from May to September

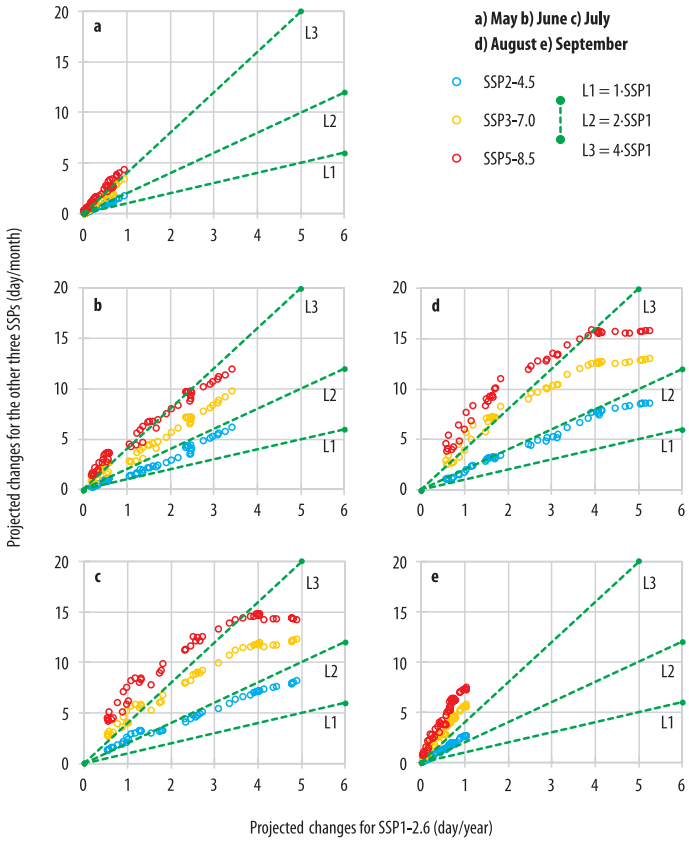

Fig. 10. Projected monthly changes of TX35 (2081–2100 vs. 1995–2014) for SSP2-4.5, SSP3-7.0 and SSP5-8.5 compared to SSP1-2.6 at 47.5°N. *Source:* Authors' own elaboration.

to the 52.5°N segment although the projected changes are even smaller here (*Figure S3*) (Supplementary section), as the minimal coefficients are identified in August. Note however, that due to the very slight projected changes, especially in May and September, the information contained in these coefficients at the 57.5°N segment is very limited.

Discussion

The trends of extreme heat events detected in the past and projected for the future have been analysed in several studies, following different approaches. For example, Cardil, A. *et al.* (2014) focused on the detected trend of air temperature at 850 hPa and high-temperature days (HTDs) in Southern Europe over the 1978–2012 period and recommended possible actions for policymakers. The main conclusion of their study is that the HTDs increased significantly in the Spanish Mediterranean Coast, Italy and Greece. The general finding of the growing risk of extreme heat events is also true for the future projections across the Mediterranean Region according to our results; however, our study area is much greater, as the above-mentioned study covers only one of the five segments of the current analysis.

A larger scale analysis for the whole European continent is given by Lorenz,

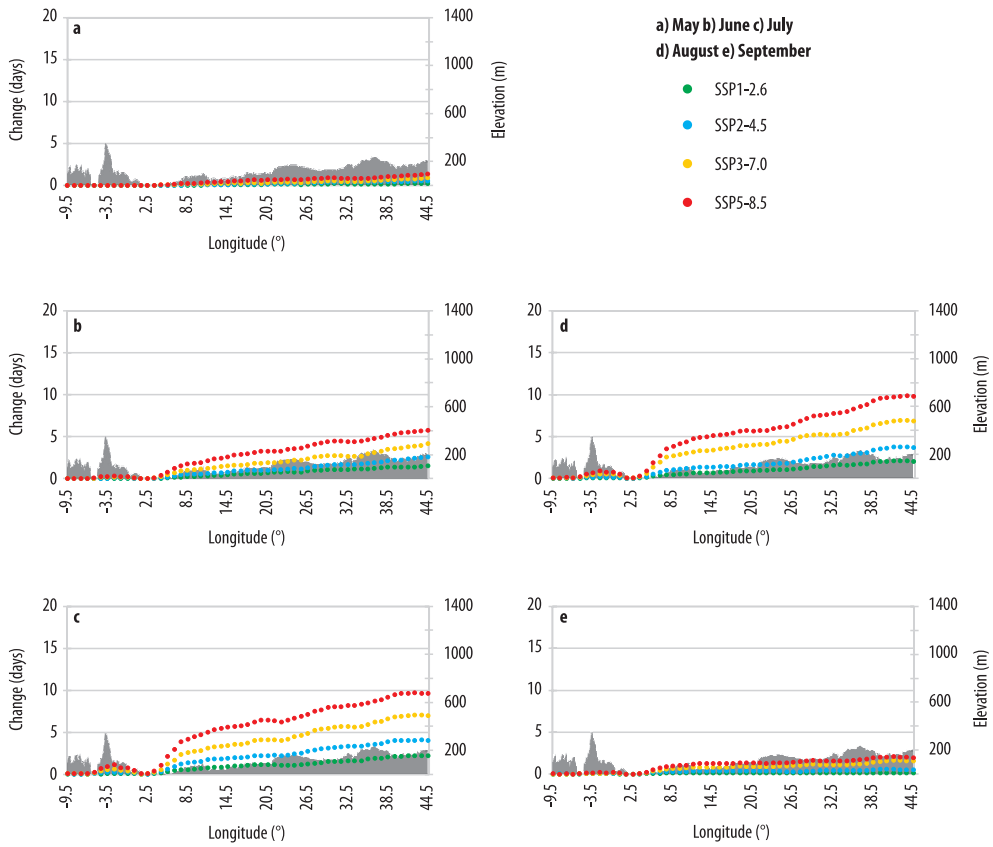

Fig. 11. Projected monthly changes of TX35 (2081–2100 vs. 1995–2014) for SSP1-2.6, SSP2-4.5, SSP3-7.0, SSP5-8.5 and elevation along the zonal segment of 52.5°N. *Source:* Authors' own elaboration.

R. *et al.* (2019), and Sulikowska, A. and Wypych, A. (2021). Both studies analysed extreme temperature increase in Europe for the past, for almost the same target period (1950–2018 and 1950–2019, respectively). However, they used slightly different datasets, Lorenz, R. *et al.* (2019) used the 4000-station data series available at the European Climate Assessment & Dataset (ECAD), whilst Sulikowska, A. and Wypych, A. (2021) used the E-OBS gridded dataset (generated from the ECAD station data) for five European subdomains. Moreover, Lorenz, R. *et al.* (2019) included both warm and cold extremes and they validated results from EURO-CORDEX simulations for their target period. Both studies' findings about increasing hot extremes resonate with our findings, however, we focused on future projections instead of past trends, for which we used the new CMIP6 simulations instead of EURO-CORDEX data where regional climate model runs were driven by the previous global models from CMIP5. Engdaw, M.M. *et al.* (2023) carried out a global analysis focusing on the frequency changes of cold and hot events for the period 1980–2020, using percentile-based climate indices instead of fix thresholds on the basis of observational data as well as simulated data from CMIP6. They found an overall significant increase in the frequency of hot events, and a decrease in

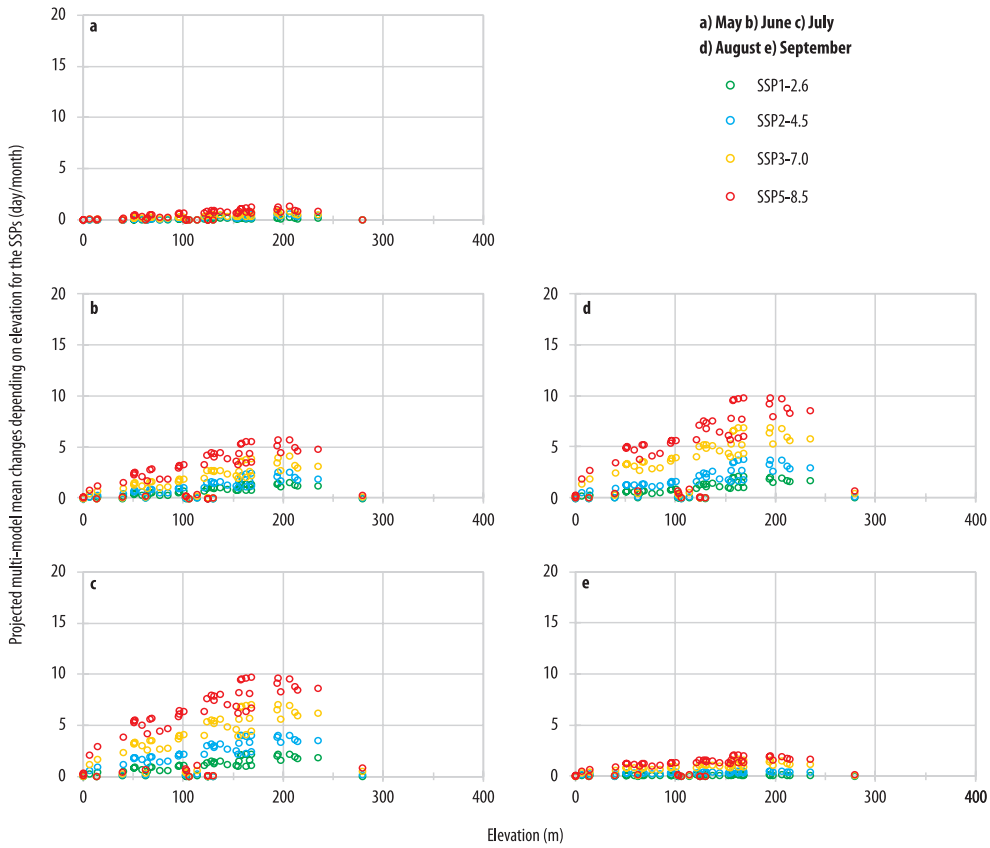

Fig. 12. Projected monthly changes of TX35 (2081–2100 vs. 1995–2014) depending on elevation at 52.5°N for SSP1-2.6, SSP2-4.5, SSP3-7.0 and SSP5-8.5. *Source:* Authors' own elaboration.

cold events for Europe, however, because the whole continent was analysed as one region, the comparison of different European areas is not possible, unlike in our study.

The studies made by Fan, X. *et al.* (2020), Alvarez, I. *et al.* (2024) and Srivastava, A.K. *et al.* (2024) all analysed both the past trends and the future changes of different temperature indices, more specifically, Fan, X. *et al.* (2020) used the CMIP6 simulations' outputs to analyse annual mean temperatures for three different past and three different future periods. Alvarez, I. *et al.* (2024), similarly to Cardil, A. *et al.* (2014), or Sulikowska, A. and Wypych, A. (2021), defined a compound heat and drought metric, the so-called Heat Index to assess the trends and projections in the Mediterranean Basin, using the CMIP6 simulations for the SSP2-4.5 and the SSP5-8.5 scenarios. On the other hand, Srivastava, A.K. *et al.* (2024) used temperature-based indices, i.e. the maximum and the mean of daily maximum temperatures to study the local hydroclimatic effects on different warming rates in the Northern Hemisphere for only one specific high emission scenario, i.e. RCP8.5. All these studies found increasing trends in their respective extreme heat indices, with Alvarez, I. *et al.* (2024) pointing out dangerous increase in heat stress over the Mediterranean. Our re-

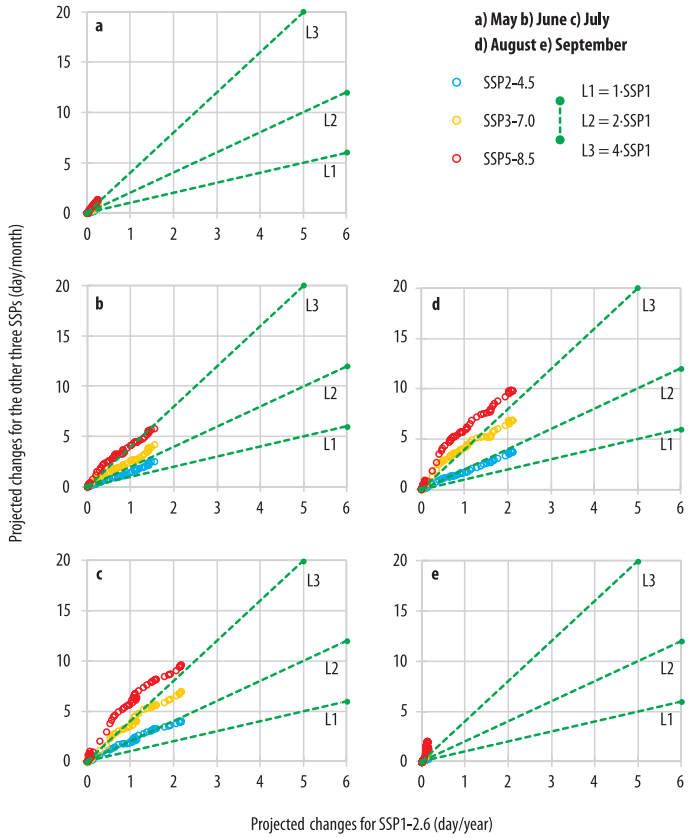

Fig. 13. Projected monthly changes of TX35 (2081–2100 vs. 1995–2014) for SSP2-4.5, SSP3-7.0 and SSP5-8.5 compared to SSP1-2.6 at 52.5°N. *Source:* Authors' own elaboration.

sults agree with these findings, however, we extended the number of scenarios taken into account, thus, providing a more systematic analysis of the projections to cover a wider range of future climatic possibilities.

A different approach was used by the studies of King, A.D. *et al.* (2018), and Tebaldi, C. and Knutti, R. (2018), who all used the time-sampling method, where instead of the analysis of a certain target period, the thresholds of global average temperature increase were set (i.e. 1.5 °C or 2 °C). Then, the exposure to extreme heat events is assessed when these certain thresholds are reached. The extreme heat indices, however, do not include TX35, and the simulations being used are from the earlier simulated data of CMIP5, using the RCP scenarios. Tebaldi, C. and Knutti, R. (2018) also analysed only the lower radiative forcing change scenarios, RCP2.6 and RCP4.5, but still, summarised similar conclusions to our study about the SSP1-2.6 and SSP2-4.5, namely, that the connections between RCP2.6 and RCP4.5 are almost linear. This is also confirmed by King, A.D. *et al.* (2018).

A limited set of CMIP6 simulations (i.e. 12 global climate models) is compared to CMIP5 simulations as well as their downscaled results of EURO-CORDEX by Coppola, E. *et al.* (2021). Their study is focusing mainly on business-as-usual scenarios (i.e. RCP8.5 and SSP5-8.5). In case of TX35, EURO-CORDEX results show an

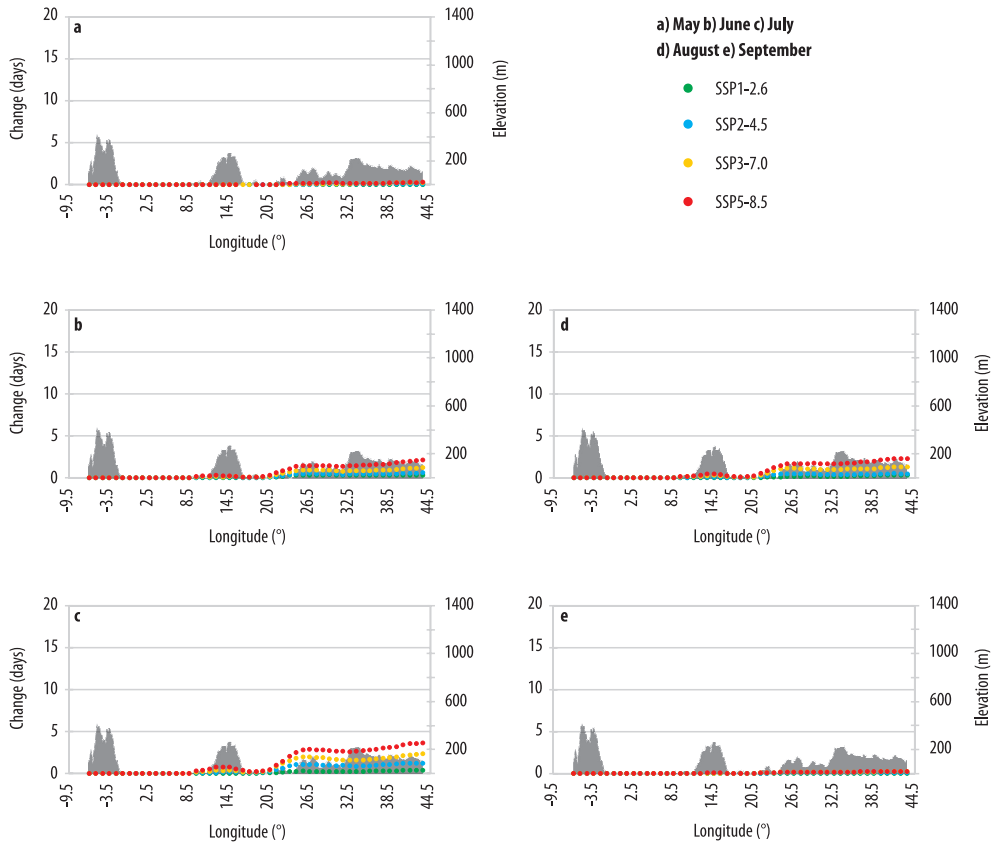

Fig. 14. Projected monthly changes of TX35 (2081–2100 vs. 1995–2014) for SSP1-2.6, SSP2-4.5, SSP3-7.0, SSP5-8.5 and elevation along the zonal segment of 57.5°N. *Source:* Authors' own elaboration.

overall smaller change compared to the driving CMIP5 simulations, however, CMIP6 simulations result in higher increase than CMIP5 simulations. This can be partly due to the coarser horizontal resolution of CMIP5 simulations (2°). Certainly, regional climate models with 0.11° horizontal resolution better represent orography, and, thus, more precise differences are simulated in temperature-related extremes, compared to the global models. Nevertheless, the overall spatial pattern of the projected changes of temperature extremes (including TX35) is similar in regional and global models. All these allow providing information on the basis of CMIP6 simulations before downscaled regional climate model simulations are available.

Suarez-Gutierrez, L. *et al.* (2023) also used a similar methodology as e.g. Wobus, C. *et al.* (2018), but instead of a temperature-threshold, the main results highlight the time by which never-seen-before heat waves and multi-year successive extremes in temperature will become common in the European continent. For this purpose, compound heat and drought metrics were used instead of selecting a particular temperature threshold and analysing the frequency changes of its exceedances over time. Despite the different approach, their results are similar to our findings as they also highlight that even a slight warming may cause huge consequences in Europe.

Overall, the future projections of CMIP6 simulations across the entirety of Europe have not been analysed in a systematic way before, so we aimed to fill this gap with visual and qualitative assessments. Most studies focus mainly on the Mediterranean region; however, our findings show that a substantial increase is projected even as north as the Baltic Sea. The results presented here contain four SSP scenarios providing the widest range of potential future climate compared to other studies carried out earlier. Furthermore, the usage of the TX35 index is not as widespread as other indices, even though it is an important threshold when analysing extreme temperature events with high heat stress. The projected occurrence of the daily maximum temperature above 35 °C is a clear warning signal in the northern parts of Europe as well, since the spatial extent of such extreme temperatures towards the polar region was much smaller in the reference period (*Figure S1*). Finally, the use of zonal segments to study the effects of sea cover, continentality or elevation is a unique and novel approach to make systematic inter-comparisons between segments or even grid points.

The main underlying causes of extreme heat occurrences in Europe are discussed in details by Andrade, C. *et al.* (2012), and Sousa, P.M. *et al.* (2018). They both analysed large-scale circulation patterns focusing on blocking and ridges over the continent. Overall, changes in the meridional pressure gradient play a major role in extreme hot conditions over Europe.

We note that there are some limitations of the present study. (i) The inter-model variability or the uncertainty from the simulations' ensemble cannot be assessed, as only the multi-model mean was available in the IPCC IA, which is the basis of the present analysis. (ii) The horizontal resolution of global climate models is quite coarse, so detailed regional specifics cannot always be properly represented. (iii) This study analysed only one specific climate index indicating the frequency of heat conditions above a fixed threshold. Even though these heat-related climate indices are interrelated they certainly have their unique approach, e.g. duration of consecutive heat conditions, intensity of heat, which are clearly not addressed by TX35. (iv) The underlying meteorological and climatological processes require further detailed analysis of large-scale circulation using pressure and wind data from CMIP6 simulations. This is beyond the aims of the current study.

Conclusions

In this study, future extreme temperature projections are analysed over Europe using the CMIP6 simulations included in the IPCC's AR6 report (i.e. in the IA) for a specific heat-related climate index, the TX35. Based on the presented analysis, the main research questions can be answered as follows.

(i) On the basis of the ensemble mean of historical simulations, the TX35 index had a distinct spatial distribution in the reference period of 1995–2014. It was an important climatic feature in the Mediterranean Region even in the recent years, with a mean monthly number of days above 35 °C reaching almost 14 in August. On the other hand, in the northern parts of Europe, there were only 1–2 days in a year on average, when the daily maximum temperature reached the 35 °C threshold.

(ii) Climate change is expected to further accentuate the spatial patterns already observed. The highest increases are projected for the southern segments (around 18 days for the 42.5°N), whereas at the most northern 57.5°N segment, very slight changes are projected (maximum of +4 days in August). This can be expected because the 35 °C threshold of daily maximum temperature is so extreme at this segment, that even the temperature increase projected by the SSP5-8.5 scenario is not high enough to reach it. Regarding the scenarios, the results clearly imply that the projections for the highest radiative forcing changes, SSP5-8.5, will lead to the greatest

increases, and therefore the greatest spatial differences between the different parts of the continent. Meanwhile, the projected changes for the lowest radiative forcing changes, the SSP1-2.6 scenario, show the smallest increases, potentially creating much smaller spatial differences than the SSP5-8.5. For instance, at the maximal increase grid point (42.5°N, 22.5°E), the projections range between +4 days (SSP1-2.6) to +18 days (SSP5-8.5). The difference of the TX35 projections is a quite straightforward consequence of the difference of global and regional warming originating from the direct link between the radiative forcing and temperature changes.

(iii) There are also several geographical effects that influence the patterns of the TX35. For instance, a greater increase is projected for the more continental (eastern) parts of the 47.5°N, 52.5°N and 57.5°N segments, which creates greater intra-zonal differences than in the reference period. For instance, at the 47.5°N, the difference in the increase of TX35 in August between the most western and eastern parts based on the SSP5-8.5 scenario is 9 days. In the southern segments, namely along 37.5°N and 42.5°N, the most important influence is the sea cover, as the increase of TX35 is much lower above the water surfaces than above the land areas (e.g. at the 42.5°N, the greatest difference is 15 days for the SSP5-8.5 scenario in August) due to the moderating climate effect of large water bodies. Finally, the height above sea level can also be an important factor, especially along the 47.5°N segment, as much lower increase is projected by the ensemble mean of the CMIP6 simulations for any scenario in the higher elevation regions than in the lower elevations. For instance, the differences can reach 12 days in August based on the SSP5-8.5 scenario. The Alps is especially important in this segment as the results show that there is a great difference in the increase of the TX35 between the sub-segments to the east and to the west from the mountainous area (except the Carpathians, which area has similar characteristics to the western part of the segment due to its higher elevation).

The potential increase of heat stress certainly is one of the major future challenges, especially in case of the more pessimistic scenarios. Therefore, in addition to mitigation efforts, adaptation is also essential in the next decades. In order to develop reliable adaptation strategies, interdisciplinary studies are necessary, which take into account not only climatological aspects, but other key factors (e.g. population, financial demand, environmental constrains) as well.

Acknowledgements: This work has been implemented by the National Multidisciplinary Laboratory for Climate Change (RRF-2.3.1-21-2022-00014) project within the framework of Hungary's National Recovery and Resilience Plan supported by the Recovery and Resilience Facility of the European Union.

REFERENCES

Alvarez, I., Diaz-Poso, A., Lorenzo, M.N. and Roye, D. 2024. Heat index historical trends and projections due to climate change in the Mediterranean basin based on CMIP6. *Atmospheric Research* 308. 107512. https://doi.org/10.1016/j.atmosres.2024.107512

Andrade, C., Leite, S.M. and Santos, J.A. 2012. Temperature extremes in Europe: Overview of their driving atmospheric patterns. *Natural Hazards and Earth System Sciences* 12. 1671–1691. https://doi.org/10.5194/nhess-12-1671-2012

Cardil, A., Molina, D.M. and Kobziar, L.N. 2014. Extreme temperature days and their potential impacts on southern Europe. *Natural Hazards and Earth System Sciences* 14. 3005–3014. https://doi.org/10.5194/nhess-14-3005-2014

Cogato, A., Meggio, F., de Antoni Migliorati, M. and Marinello, F. 2019. Extreme weather events in agriculture: A systematic review. *Sustainability* 11. (9): 2547. https://doi.org/10.3390/su11092547

C3S 2025. *The 2024 Annual Climate Summary: Global Climate Highlights 2024.* Copernicus Climate Change Services (C3S). Available at https://climate.copernicus.eu/global-climate-highlights-2024

Coppola, E., Nogherotto, R., Ciarlo, J.M., Giorgi, F., van Meijgaard, E., Kadygrov, N., Iles, C., Corre, L., Sandstad, M., Somot, S., Nabat, P., Vautard, R., Levavasseur, G., Schwingschackl, C., Sillmann, J., Kjellström, E., Nikulin, G., Aalbers, E., Lenderink, G., Christensen, O.B., Boberg, F., Sorland, S.L., Demory, M-E., Bülow, K., Teichmann, C., Warrach-Sagi, K. and Wulfmeyer, V. 2021. Assessment of the European climate projections as simulated by the

large EURO-CORDEX regional and global climate model ensemble. *Journal of Geophysical Research: Atmospheres* 126. (4): e2019JD032356. https://doi.org/10.1029/2019JD032356

Engdaw, M.M., Steiner, A.K., Hegerl, G.C. and Ballinger, A.P. 2023. Attribution of observed changes in extreme temperatures to anthropogenic forcing using CMIP6 models. *Weather and Climate Extremes* 39. 100548. https://doi.org/10.1016/j.wace.2023.100548

Eyring, V., Bony, S., Meehl, G.A., Senior, C.A., Stevens, B., Stouffer, R.J. and Taylor, K.E. 2016. Overview of the Coupled Model Intercomparison Project Phase 6 (CMIP6) experimental design and organization. *Geoscientific Model Development* 9. 1937–1958. https://doi.org/10.5194/gmd-9-1937-2016

Eyring, V., Gentine, P., Camps-Valls, G., Lawrence, D.M. and Reichstein, M. 2024. AI-empowered next-generation multiscale climate modelling for mitigation and adaptation. *Nature Geoscience* 17. 963–971. https://doi.org/10.1038/s41561-024-01527-w

Fan, X., Duan, Q., Shen, C., Wu, Y. and Xing, C. 2020. Global surface air temperatures in CMIP6: Historical performance and future changes. *Environmental Research Letters* 15. (10): 104056. https://doi.org/10.1088/1748-9326/abb051

Gallo, E., Quijal-Zamorano, M., Méndez Turrubiates, R.F., Tonne, C., Basagaña, X., Achebak, H. and Ballester, J. 2024. Heat-related mortality in Europe during 2023 and the role of adaptation in protecting health. *Nature Medicine* 30. 3101–3105. https://doi.org/10.1038/s41591-024-03186-1

Gutiérrez, J.M., Jones, R.G., Narisma, G.T., Alves, L.M., Amjad, M., Gorodetskaya, I.V., Grose, M., Klutse, N.A.B., Krakovska, S., Li, J., Martínez-Castro, D., Mearns, L.O., Mernild, S.H., Ngo-Duc, T., van den Hurk, B. and Yoon, J.-H. 2021. Atlas. In *Climate Change 2021: The Physical Science Basis. Contribution of Working Group I to the Sixth Assessment Report of the Intergovernmental Panel on Climate Change.* Eds.: Masson-Delmotte, V., Zhai, P., Pirani, A., Connors, S.L., Péan, C., Chen, Y., Goldfarb, L., Gomis, M.I., Matthews, J.B.R., Berger, S., Huang, M., Yelekçi, O., Yu, R., Zhou, B., Lonnoy, E., Maycock, T.K., Waterfield, T., Leitzell, K. and Caud, N., Cambridge, UK and New York, NY, USA, Cambridge University Press, 1927–2058. https://doi.org/10.1017/9781009157896.021. Interactive Atlas available from IPCC WGI Interactive Atlas

IPCC 2021. *Climate Change 2021: The Physical Science Basis. Contribution of Working Group I to the Sixth Assessment Report of the Intergovernmental Panel on Climate Change*. Eds.: Masson-Delmotte, V., Zhai, P., Pirani, A., Connors, S.L., Péan, C., Berger, S., Caud, N., Chen, Y., Goldfarb, L., Gomis, M.I., Huang, M., Leitzell, K., Lonnoy, E., Matthews, J.B.R., Maycock, T.K., Waterfield, T., Yelekçi, O., Yu, R. and Zhou, B., Cambridge, UK and New York, NY, USA, Cambridge University Press. https://doi.org/10.1017/9781009157896

King, A.D., Knutti, R., Uhe, P., Mitchell, D.M., Lewis, S.C., Arblaster, J.M. and Freychet, N. 2018. On the linearity of local and regional temperature changes from 1.5 °C to 2 °C of global warming. *Journal of Climate* 31. 7495–7514. https://doi.org/10.1175/JCLI-D-17-0649.1

Lorenz, R., Stalhandske, Z. and Fischer, E.M. 2019. Detection of a climate change signal in extreme heat, heat stress, and cold in Europe from observations. *Geophysical Research Letters* 46. (14): 8363–8374. https://doi.org/10.1029/2019GL082062

Lüthi, S., Fairless, C., Fischer, E.M., Scovronick, N., Armstrong, B., de Sousa Zanotti Stagliorio Coelho, M., Guo, Y.L., Guo, Y., Honda, Y., Huber, V., Kyselý, J., Lavigne, E., Royé, D., Ryti, N., Silva, S., Urban, A., Gasparrini, A., Bresch, D.N., Vicedo-Cabrera, A.M. and Multi-Country Multi-City (MCC) Collaborative Research Network 2023. Rapid increase in the risk of heat-related mortality. *Nature Communications 14.* (1): 4894. https://doi.org/10.1038/s41467-023-40599-x

O'Neill, B.C., Kriegler, E., Ebi, K.L., Kemp-Benedict, E., Riahi, K., Rothman, D.S., van Ruijven, B.J., van Vuuren, D.P., Birkmann, J., Kok, K., Levy, M. and Solecki, W. 2017. The roads ahead: Narratives for shared socioeconomic pathways describing world futures in the 21st century. *Global Environmental Change* 42. 169–180. https://doi.org/10.1016/j.gloenvcha.2015.01.004

Rojas-Downing, M.M., Nejadhashemi, A.P., Harrigan, T. and Woznicki, S.A. 2017. Climate change and livestock: Impacts, adaptation, and mitigation. *Climate Risk Management* 16. 145–163. https://doi.org/10.1016/j.crm.2017.02.001

Schaeffer, R., Szklo, A.S., de Lucena, A.F.P., Borba, B.S.M.C., Nogueira, L.P.P., Fleming, F.P., Troccoli, A., Harrison, M. and Boulahya, M.S. 2012. Energy sector vulnerability to climate change: A review. *Energy* 38. (1): 1–12. https://doi.org/10.1016/j.energy.2011.11.056

Sousa, P.M., Trigo, R.M., Barriopedro, D., Soares, P.M. and Santos J.A. 2018. European temperature responses to blocking and ridge regional patterns. *Climate Dynamics* 50. 457–477. https://doi.org/10.1007/s00382-017-3620-2

Srivastava, A.K., Wehner, M., Bonfils, C., Ullrich, P.A. and Risser, M. 2024. Local hydro-climate drives differential warming rates between regular summer days and extreme hot days in the Northern Hemisphere. *Weather and Climate Extremes* 45. 100709. https://doi.org/10.1016/j.wace.2024.100709

Suarez-Gutierrez, L., Müller, W.A. and Marotzke, J. 2023. Extreme heat and drought typical of an end-of-century climate could occur over Europe soon and repeatedly. *Communications Earth and Environment* 4. (1): 415. https://doi.org/10.1038/s43247-023-01075-y

Sulikowska, A. and Wypych, A. 2021. Seasonal variability of trends in regional hot and warm temperature extremes in Europe. *Atmosphere* 12. (5): 612. https://doi.org/10.3390/atmos12050612

Taylor, K.E., Stouffer, R.J. and Meehl, G.A. 2012. An overview of CMIP5 and the experiment design. *Bulletin of the American Meteorological Society* 93. 485–498. https://doi.org/10.1175/BAMS-D-11-00094.1

Tebaldi, C. and Knutti, R. 2018. Evaluating the accuracy of climate change pattern emulation for low warming targets. *Environmental Research Letters* 13. (5): 055006. https://doi.org/10.1088/1748-9326/aabef2

van Vuuren, D.P., Edmonds, J., Kainuma, M., Riahi, K., Thomson, A., Hibbard, K., Hurtt, G.C., Kram, T., Krey, V., Lamarque, J-F., Masui, T., Meinshausen, M., Nakicenovic, N., Smith, S.J. and Rose, S.K. 2011. The representative concentration pathways: An overview. *Climatic Change* 109. 5–31. https://doi.org/10.1007/s10584-011-0148-z

Wilks, D.S. 2006. *Statistical Methods in the Atmospheric Sciences*. 2nd edition. London, Academic Press.

WMO 2025. *State of the Global Climate in 2024*. WMO-No. 1368. Geneva, WMO.

Wobus, C., Zarakas, C., Malek, P., Sanderson, B., Crimmins, A., Kolian, M., Sarofim, M. and Weaver, C.P. 2018. Reframing future risks of extreme heat in the United States. *Earth's Future* 6. (9): 1323–1335. https://doi.org/10.1029/2018EF000943

Supplementary section

*Table S1. The list of simulations included in the multi-model ensemble of the IA for the different scenarios**

Models	SSP1-2.6	SSP2-4.5	SSP3-7.0	SSP5-8.5
ACCESS-CM2_r1i1p1f1	✓	✓	✓	✓
ACCESS-ESM1-5_r1i1p1f1	✓	✓	✓	✓
AWI-CM-1-1-MR_r1i1p1f1	✓	✓	✓	✓
BCC-CSM2-MR_r1i1p1f1	✓	✓	✓	✓
CanESM5_r1i1p1f1	✓	✓	✓	✓
CNRM-CM6-1_r1i1p1f2	✓	✓	✓	✓
CNRM-CM6-1-HR_r1i1p1f2	✓	–	–	✓
CNRM-ESM2-1_r1i1p1f2	✓	✓	✓	✓
EC-Earth3_r1i1p1f1	✓	✓	✓	✓
EC-Earth3-Veg_r1i1p1f1	✓	✓	✓	✓
EC-Earth3-Veg-LR_r1i1p1f1	–	✓	✓	–
FGOALS-g3_r1i1p1f1	✓	✓	✓	✓
GFDL-CM4_r1i1p1f1	–	✓	–	✓
GFDL-ESM4_r1i1p1f1	✓	✓	✓	✓
HadGEM3-GC31-LL_r1i1p1f3	✓	✓	–	✓
INM-CM4-8_r1i1p1f1	✓	✓	✓	✓
INM-CM5-0_r1i1p1f1	✓	✓	✓	✓
IPSL-CM6A-LR_r1i1p1f1	✓	✓	✓	✓
KACE-1-0-G_r2i1p1f1	✓	✓	✓	✓
KIOST-ESM_r1i1p1f1	✓	✓	–	✓
MIROC-ES2L_r1i1p1f2	✓	✓	✓	✓
MIROC6_r1i1p1f1	✓	✓	✓	✓
MPI-ESM1-2-HR_r1i1p1f1	✓	✓	✓	✓
MPI-ESM1-2-LR_r1i1p1f1	✓	✓	✓	✓
MRI-ESM2-0_r1i1p1f1	✓	✓	✓	✓
NESM3_r1i1p1f1	✓	✓	–	✓
NorESM2-MM_r1i1p1f1	✓	✓	✓	✓
UKESM1-0-LL_r1i1p1f2	✓	✓	✓	✓

*Note that the most simulations (27) are available for the SSP2-4.5 and SSP5-8.5 scenarios, whereas the least for the SSP3-7.0 (23).

Table S2. Correlation coefficients of the projected monthly changes along the different zonal segments between SSP1-2.6 and the other three scenarios, SSP2-4.5, SSP3-7.0, and SSP5-8.5.

Zone	SSP2-4.5				
Segments	May	June	July	August	September
37.5°N	0.91	0.99	0.97	0.97	0.99
42.5°N	0.91	0.97	0.97	0.98	0.92
47.5°N	0.97	0.97	0.99	0.99	0.98
52.5°N	0.93	0.99	0.99	0.99	0.84
57.5°N	0.83	0.98	0.97	0.87	0.74
SSP3-7.0					
Segments	May	June	July	August	September
37.5°N	0.95	0.97	0.80	0.80	0.95
42.5°N	0.91	0.94	0.93	0.93	0.87
47.5°N	0.96	0.98	0.96	0.93	0.97
52.5°N	0.93	0.99	0.98	0.96	0.80
57.5°N	0.89	0.97	0.98	0.90	0.71
SSP5-8.5					
Segments	May	June	July	August	September
37.5°N	0.93	0.97	0.75	0.70	0.96
42.5°N	0.83	0.94	0.88	0.87	0.82
47.5°N	0.96	0.98	0.96	0.96	0.85
52.5°N	0.98	0.98	0.96	0.96	0.85
57.5°N	0.82	0.95	0.98	0.94	0.65

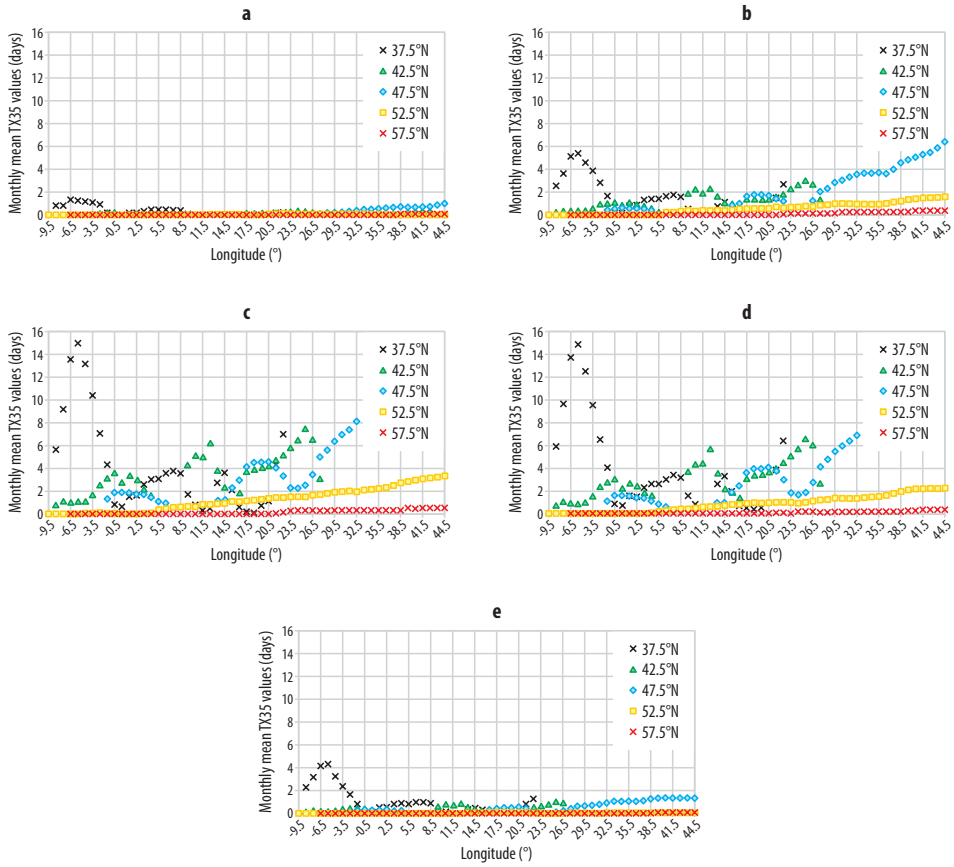

Fig. S1. Average monthly values of TX35 in the reference period 1995–2014 based on the historical CMIP6 simulations ensemble: a) May, b) June, c) July, d) August, e) September. *Source:* Authors' own elaboration.

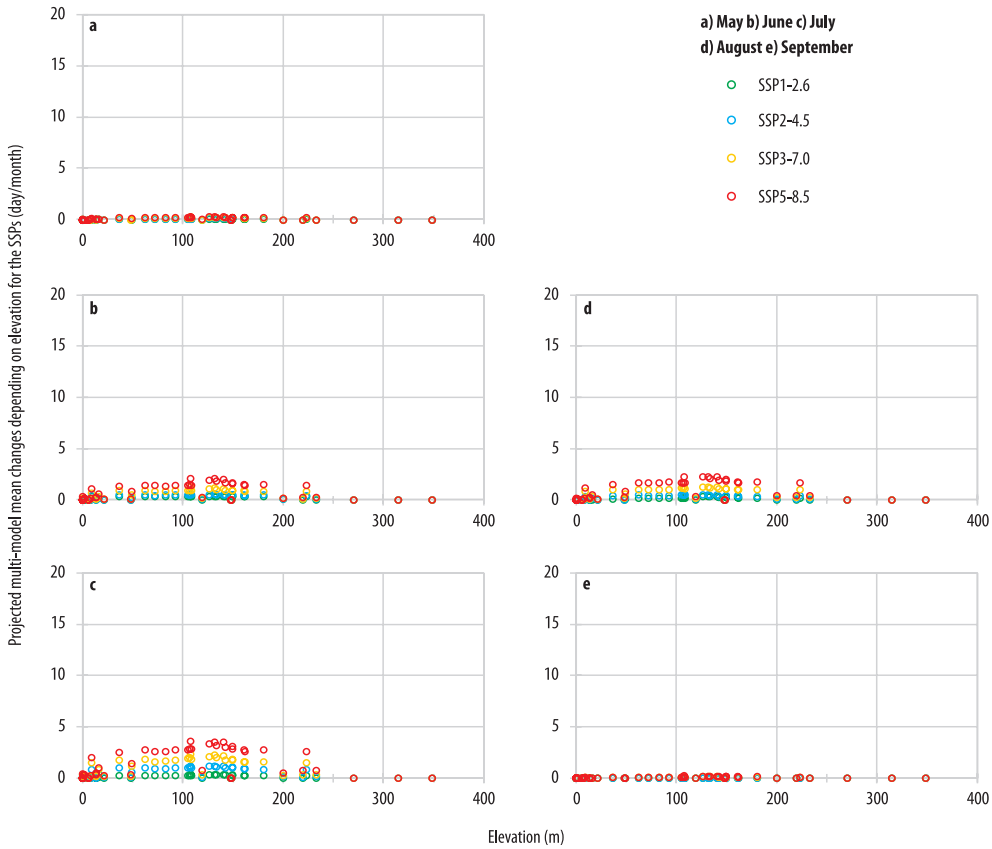

Fig. S2. Projected monthly changes of TX35 depending on elevation at 57.5°N for SSP1-2.6, SSP2-4.5, SSP3-7.0 and SSP5-8.5. *Source:* Authors' own elaboration.

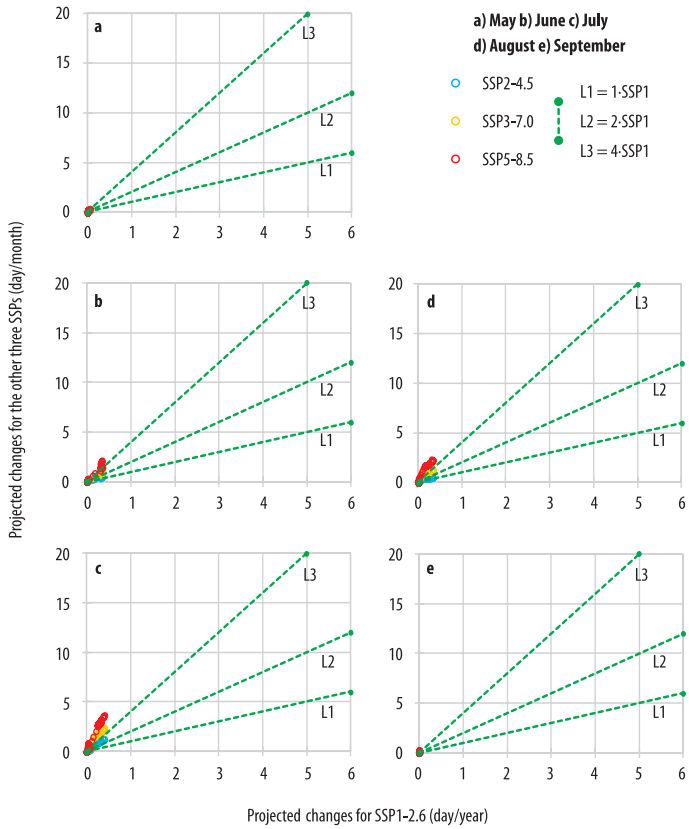

Fig. S3. Projected monthly changes of TX35 for SSP2-4.5, SSP3-7.0, and SSP5-8.5 compared to SSP1-2.6 at 57.5°N. *Source:* Authors' own elaboration.